International Journal of Hydrogen Energy 105 (2025) 492–504

Contents lists available at ScienceDirect

International Journal of Hydrogen Energy

journal homepage: www.elsevier.com/locate/he

Underground hydrogen storage in sandstone reservoirs: Effects of geochemical reactivity of hydrogen on reservoir performance

Chaojie Cheng *, Benjamin Busch, Agnes Kontny, Christoph Hilgers

Structural Geology & Tectonics, Institute of Applied Geosciences, KIT Karlsruhe Institute of Technology, Adenauerring 20a, 76131, Karlsruhe, Germany

ARTICLE INFO

Handling Editor: Dr A Bhatnagar

Keywords:
Underground hydrogen storage
Buntsandstein sandstones
Geochemical reactions
Batch experiments
Reservoir performance

ABSTRACT

Underground hydrogen storage in porous rocks is a promising method to stabilize renewable energy fluctuations. However, data on the geochemical reactivity of hydrogen with reservoir rocks and its potential effects on reservoir performance are limited. This study investigates the geochemical reactivity of hydrogen with Buntsandstein reservoir sandstones from northern Germany, collected at a depth of about 2.5 km. Experiments were performed at 100 °C and 150 bar hydrogen partial pressure for four weeks, examining scenarios with dry hydrogen, synthetic saline fluid with hydrogen, synthetic saline fluid with helium (as a control), and an oxidation environment (air). We measured permeability, porosity, magnetic susceptibility, and fluid element concentration before and after the experiments. Results showed no significant mineral changes attributed to hydrogen. Magnetic susceptibility indicated no formation of magnetic minerals, such as magnetite and pyrrhotite. Minor variations in permeability and porosity were attributed to anhydrite dissolution from fluid chemistry nonequilibrium. Overall, our findings suggest hydrogen interactions with Buntsandstein sandstone (no pyrite content) at temperatures up to 100 °C do not risk hydrogen loss or reservoir performance degradation.

1. Introduction

Hydrogen is of significant importance for the decarbonization of the economy, not only because of green hydrogen produced by electrolysis but also due to the potential large-scale occurrence of natural hydrogen [1–3]. Hydrogen as an energy carrier can be converted from renewable power to balance the fluctuation of solar/wind power generation and the demand of the customers [1,4]. Technically, porous reservoirs offer a greater potential for hydrogen storage compared to salt caverns due to their widespread occurrence in sedimentary basins and their capacity to hold giant volumes [5]. However, large-scale hydrogen porous storage still faces major scientific challenges [6], including hydrogen loss and contamination due to microbial reactions [7–10], hydrogen flow through porous media [11,12], wettability [13,14], and solubility [15] of hydrogen in porous rocks, as well as rock property changes induced by geochemical reactions [16].

There are tremendous reviews summarizing that microbial reactions are supposed to be the major problem for hydrogen storage since hydrogen is the universal electron donor for many microbial metabolisms, which will consume and convert hydrogen to other forms (e.g., H_2S and methane) [17–19]. However, hydrogen is also the electron donor for many abiotic geochemical reactions [20–23], such as reactions with pyrite [24], sulphates [25], iron oxides (e.g, hematite) [26,27], and carbonates [28–30]. Most of the above geochemical reactions require elevated temperatures at least higher than 200 °C in the absence of water, where the reaction may occur directly on the gas-solid interfaces, such as calcite (>500 °C) [28,29], hematite (>200 °C) [26,27], and pyrite (>250 °C) [24,31]. A recent study discovered that reduction of iron-bearing minerals such as pyrite, hematite, iron-bearing clays (like smectite), and anhydrite can occur at 120 °C and 200 bar in hydrogen pressure. However, significant amounts of reduction were observed only with pyrite and hematite [32,33]. In addition, a small portion of the structural Fe(III) in synthetic montmorillonite-type clays can be reduced by the adsorbed hydrogen gas under dry conditions, via $2Fe^{3+} + H_2 \rightarrow 2Fe^{2+} + 2H^+$ [34]. Therefore, it is noticed that temperature is the primary factor determining the reactivity of hydrogen with these minerals.

In the presence of water, reactions will depend on aqueous hydrogen ($H_2 = 2H^+ + e^-$) associated with hydrogen dissolution and dissociation [15,35,36]. The required temperatures for initiating hydrogen-fluid-mineral reactions are commonly lower than those in dry conditions. For instance, pyrite to pyrrhotite reduction in calcite-buffered solutions can occur at a temperature as low as 90 °C [37,

* Corresponding author.
E-mail address: chaojie.cheng@kit.edu (C. Cheng).

https://doi.org/10.1016/j.ijhydene.2025.01.330
Received 6 August 2024; Received in revised form 3 January 2025; Accepted 21 January 2025
Available online 25 January 2025

38]. Aqueous sulphate can be reduced at 250–300 °C with negligible effects on hydrogen partial pressure between 4 and 16 bar [25], but with the requirement of H_2S as the catalyst for the reactive intermediates [39]. Research on calcite reaction with hydrogen in aqueous conditions remains inconsistent across experiments and between experimental results and theoretical models. One experimental study indicated that calcite dissolution in claystone caprock can be enhanced in the conditions of the hydrogen-brine mixture at room temperature for 30 days, which implies the hydrogen dissociation-facilitated dissolution mechanism [40]. Al-Yaseri et al. [41] reported a significant calcite expansion under a hydrogen-brine environment at 75 °C over 75 days, causing a porosity reduction of 50% (CT model-based analysis). However, Al-Yaseri et al. [42] conducted a similar study on the interaction between limestone and hydrogen under comparable conditions but did not find significant effects on porosity and gas composition. Additionally, a batch experiment with pure calcite was performed under a hydrogen-brine saturated environment at 100 bar hydrogen partial pressure and a temperature of 105 °C, demonstrating the non-reactive behavior of calcite with hydrogen [43]. Conversely, numerous geochemical modeling studies using PHREEQC have shown substantial calcite dissolution and methane production over decades due to calcite-hydrogen reactions [35,36,44]. There is a notable disparity among various modeling and experimental studies regarding whether geochemical reactions occur and their impact on reservoir properties.

While the reactivity of pure minerals with hydrogen has been extensively studied, ongoing debates still exist. Rare experiments investigate hydrogen reactivity with natural bulk rocks, but understanding its potential effects on rock petrophysical properties is crucial for reservoir assessment. Potential hydrogen reactions may not only consume or contaminate hydrogen but also convert mineral phases affecting petrophysical properties. While limited studies have explored the reactivity of sandstones with hydrogen, the findings remain inconclusive [16,45–47]. Notably, Flesch et al. [16] investigated the impact of potential hydrogen reactions under saturated conditions on porosity, permeability, and effective surface area of bulk samples, revealing minor effects on reservoir performance. These findings suggest that reaction rates determined from experiments using powders with particle sizes in the μm to nm range might not directly translate to natural rock systems. This discrepancy is likely due to the inherent complexity of natural rocks, which includes a diverse mineral composition, a range of mineral grain sizes, variable surface areas available for reaction, and differing effective pore space configuration among other factors.

Importantly, the presence or absence of water has a detectable influence on hydrogen-mineral reactions with different reactive mechanisms, i.e., gas-solid interface reactions [26,29,31] and dissociated hydrogen-facilitated mineral reactions [25,37,43]. This is also applicable in reservoirs because gas injection into saline aquifers or reservoirs forms a dry-out zone, a partially-saturated two-phase zone, and a saturated zone, where gas may dissolve. Dry and wet conditions have seldom been systematically explored in batch experiments for assessing rock petrophysical properties [46]. To accurately identify reactions specifically associated with hydrogen, it is essential to conduct control reference experiments, such as those using inert gases.

In this study, we investigate potential geochemical reactions between drill cores (Triassic Buntsandstein reservoir sandstones from a depth of about 2500 m) and hydrogen under dry and wet conditions. Porosity, permeability, petrographic properties, magnetic susceptibility, and fluid element concentration were measured before and after the batch experiments. We also conducted control tests using inert helium gas. This approach allows us to systematically identify the specific causes of the results with a baseline. We can thus determine whether the changes are due to pure fluid-rock interaction, thermal effects alone, reactions at the hydrogen-mineral interface, or mineral dissolution facilitated by dissociated hydrogen.

2. Materials and methods

The methodology and experimental apparatuses used in this study are illustrated in Fig. 1. The workflow includes sample and fluid preparation, as well as the analytical analysis of samples before and after the alteration experiments. A more detailed description is provided below.

2.1. Rock materials

The samples were obtained from drill cores in a gas field located in northern Germany. The sandstones (Triassic Buntsandstein reservoir sections) at a depth of about 2.5 km were selected for preparing cylindrical samples with a diameter of 25 mm and a length of about 40 mm. In addition to porous and permeable sandstones, low permeable sequences of shaly sandstone, sandy shale, and shale interlayers can be found in the formation. We selected relatively high permeable samples for our experiments. All 11 cylindrical specimens named BS1 to BS11 are perpendicular to the longitudinal axis of the drill cores (i.e. parallel to sediment stratification). The trim ends of each cylindrical specimen are used for thin section preparation for the petrographic analysis of the initial material as shown in Fig. 1a. Trim ends are embedded in blue-dyed epoxy resin, fixed on a glass slide, and ground to a final thickness of approx. 30 μm. Before covering with a glass coverslip, samples are half-stained using a combined Alizarin red S and Potassium ferricyanide solution [48] to aid the assessment of carbonate mineral phases. Subsequently, thin sections of altered samples after batch experiments were prepared for the observation of potential corroded mineral phases, in comparison with the initial materials. This will provide us with a semi-quantitative comparison of potential reactive minerals.

2.2. Synthetic formation fluid

The synthetic fluid was prepared using rock samples, to achieve a solution that is in chemical equilibrium with the sandstone samples at experimental conditions. The fluid was used for the alteration experiments, to minimize potential pure geochemical reactions between rock specimens and the fluid. Some remaining sample materials, i.e., 7.41 g from BS6 and 4.39g from BS8 leftovers, were crushed into fine powders and put into a glass bottle (i.e., pressure plus screw top bottle DURAN) filled with 1 L of pure water (i.e., electrical resistivity is about 18 MΩ × cm at room temperature) for the synthetic fluid preparation (Fig. 1a). The bottle is sealed by a rubber stopper and a thermocouple is punched through the stopper into the fluid to measure the temperature in the bottle. The bottle is put on a magnetic heating plate with a magnetic stirrer bar inside to stir the fluid under a constant temperature of 90 °C for four days. When compared to the actual measured composition of the formation fluid in the gas field, the prepared solution is deficient in Na. Consequently, after rock dissolution and filtering, we added 8% sodium chloride (NaCl) to achieve an elevated NaCl concentration. The purpose is to prepare a solution that closely resembles the chemical equilibrium found in the in-situ environment.

2.3. Analytical methods

Rock and fluid samples were analyzed before and after the batch experiments. The analyses included petrographic observation, porosity and permeability measurements, magnetic susceptibility, and fluid element concentration as illustrated in Fig. 1a.

Petrographic analysis: Thin sections of all samples before and after the batch experiments were prepared for optical microscopy observation under transmitted and crossed-polarized lights to find potential altered mineral phases. Additionally, modal proportions of mineral phases in initial samples were determined with a semi-automatic point counter [49,50].

Petrophysical properties: Porosity and permeability were measured before and after the batch experiments. All cylindrical samples were

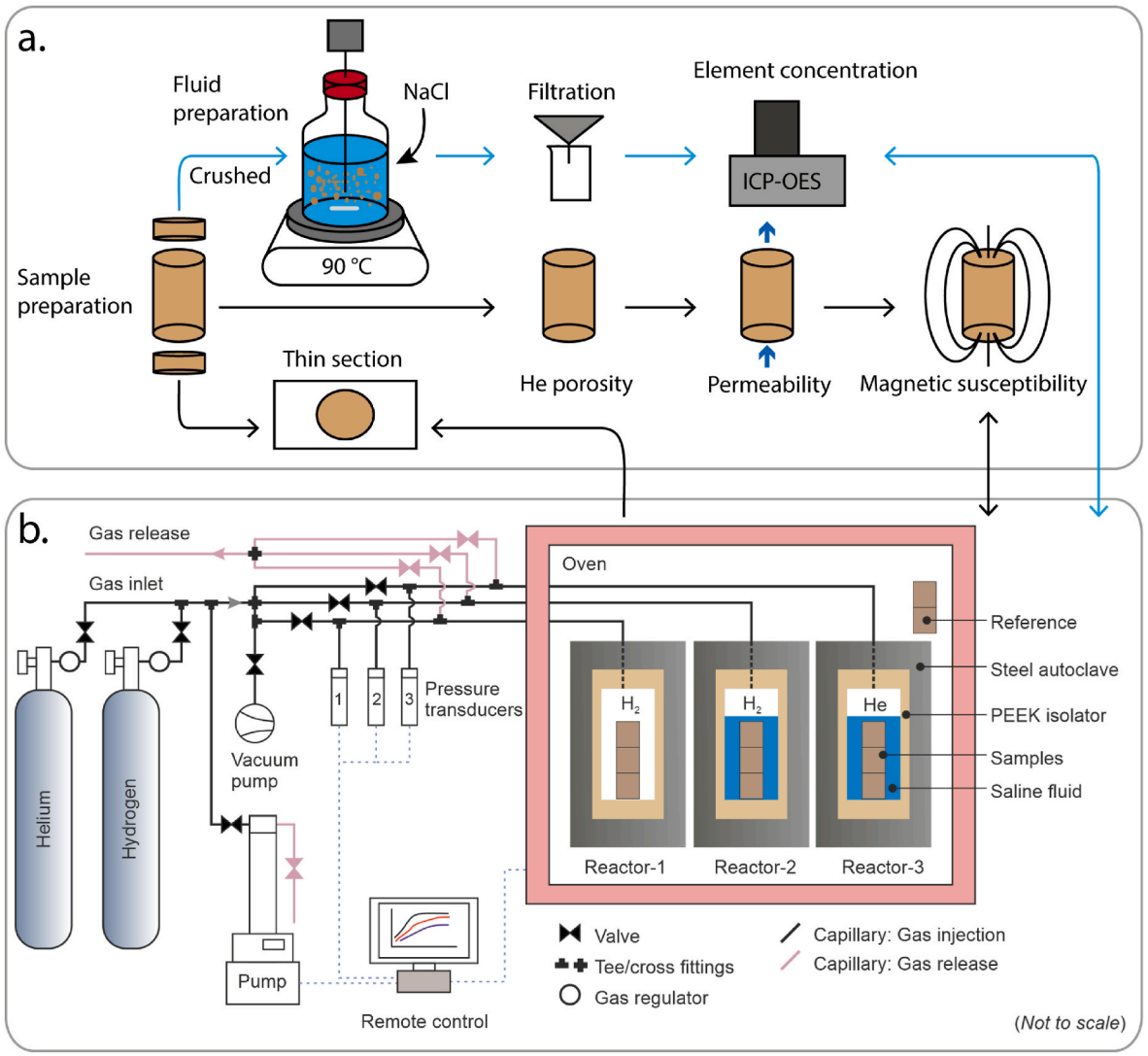

Fig. 1. a. Methodology workflow detailing sample/fluid preparation and analytical methods used in this study. b. Sketch of static batch reactors used for hydrogen alteration experiments, including three reactors connected in parallel with hydrogen and helium cylinders.

dried in an oven at 40 °C for two days before any petrophysical measurements. The solid phase volume of the samples was measured with a helium pycnometer (Micromeritics, AccuPyc II 1340), and porosity was derived with known dimensions of the cylindrical specimens. Additionally, the Klinkenberg-corrected permeability [51] of rock specimens was measured using an air permeameter (Westphal Mechanik) with steady-state flow under a confining pressure of 1.2 MPa, using dry, oil-free lab air as permeant. The setup achieves an error margin of less than 0.1% of the final permeability value, and the measurements are reproducible within an average deviation of 1.8% from the reported values [52].

Magnetic susceptibility: Magnetic susceptibility serves as an indicator for detecting potential mineral reactions, including the transformation of hematite/goethite to magnetite/iron and pyrite to pyrrhotite/troilite, or vice versa. Magnetite shows magnetic susceptibility orders of magnitude higher than hematite/goethite, and even traces of hematite/goethite that are reduced will result in significantly increased magnetic susceptibility values [53]. Pyrite is a non-magnetic mineral, whereas ferrimagnetic pyrrhotite (Fe_7S_8) is stronger magnetic compared to pyrite [54]. Therefore, changes in the magnetic susceptibility of samples before and after the batch experiments yield valuable insights into potential magnetic mineral formation (e.g., magnetite, iron, and pyrrhotite). The magnetic susceptibility of all samples before and after the batch experiments was measured at room temperature using an AGICO Kappabridge KLY-4S in a magnetic field of 300 A/m and an operating frequency of 875 Hz. Each sample was measured three times by counting the mean to ensure the accuracy of the measurement. We calculated the mass-normalized susceptibility, χ (m^3/kg) for a systematic comparison, which can be derived as,

$$\chi = \frac{V_0}{m} k \tag{1}$$

where m is specimen mass and k is the volume susceptibility, given by the Kappabridge for a nominal volume of the instrument of $V_0 = 10\ cm^3$.

Fluid chemistry: The prepared synthetic initial fluid and the fluids after the batch experiments were sampled and acidified with 1 % HNO_3 for ICP-OES (iCap 7000, Thermo Fisher) and IC measurements at the Laboratory for Environmental and Raw Materials Analysis (LERA) at the Institute of Applied Geosciences, KIT. Na, Ca, K, Fe, Sr, Mg, Ba, Li, B, Al, Mn, As, Rb, Pb, and Si were detected. The initial fluid contains 46.8 g/L Cl, 2.1 mg/L bromide, 3.7 mg/L nitrate, and 554.0 mg/L sulphate, respectively. Carbonate concentration (CO_3^{2-}) is sensitive to temperature and pressure, thus not included in the measurements. The pH of the fluid before and after the experiments was measured with a pH indicator strip.

2.4. Experimental apparatus

Three corrosion-resistant batch reactors were built and used for the batch experiments, as depicted in Fig. 1b. These reactors are engineered to withstand a maximum pressure of 300 bar and are housed in an oven (Memmert UF110) with a maximum heating capacity of up to 300 °C. Two gas cylinders containing pure hydrogen and helium are connected in parallel with all reactors. Additionally, three pressure transducers (i.e., KELLER, 23SX/0–250 bar) are in line to measure the actual pressure within each reactor. The setup includes a high-pressure syringe pump (Teledyne ISCO 260X) and a vacuum pump (CRVpro 4) to pressurize or vacuum the system, respectively. Pressure and temperature can be monitored and recorded by the dedicated control software. The batch reactors are composed of an inner PEEK isolator housed in a stainless steel (Hastelloy) autoclave.

For a standard sample assembly, the whole system is vacuumed completely for 2 h. Subsequently, gas is introduced into the syringe pump at a relatively low pressure of 10 bar and then pressurized to the target pressure of 150 bar by the pump stepwise. Multiple stages of pressurization may be required to achieve the desired target pressure due to the high compressibility of the gas. Utilizing the pump to maintain and adjust the actual pressure in the reactor ensures a minimal volume of hydrogen in the pipeline system, thereby reducing the risk of leakage from the high-pressure gas cylinders. This apparatus enables the execution of experiments under constant volume or constant pressure conditions. Additionally, a hydrogen detector (i.e., SENKO SGT portable hydrogen-gas detector, 0–1000 ppm) is used to detect and monitor any potential hydrogen leakage in the system, ensuring operational safety.

2.5. Experimental procedures

To differentiate the potential reactions facilitated by hydrogen rather than pure fluid-rock interactions or other thermal effects on samples, we conducted four scenarios of experimental conditions for comparison. These include 1) pure hydrogen, 2) pure hydrogen + synthetic fluid, 3) helium + synthetic fluid, and 4) air (Table 1 and Fig. 1b). The latter two are control tests designed to confirm any potential changes in rock properties that may result from nonequilibrium of fluid chemistry and the effect of heating in an oxidative environment, respectively. Helium is an inert gas with a low solubility in water, which was used as a reference in comparison to hydrogen.

Using the synthetic fluid, samples BS4 – BS9 were vacuum-saturated in a desiccator for three days. Subsequently, dry samples BS1 – BS3 and brine-saturated samples were moved into the reactors, which were assembled and sealed. Each reactor was thoroughly evacuated to remove any oxygen, and then it was filled with the corresponding gas. Reactors were pressurized to about 130 bar at room temperature and heated to 100 °C with all valves remaining closed. The inner pressure of the reactors was increased by heating and adjusted precisely afterwards using the ISCO pump to achieve 150 bar. The pressures were recorded continuously by the transducers with a total experimental duration of approximately 28 days.

Table 1
Physico-chemical conditions of the four batch experiments.

Reactor No.	Samples	Gas	Fluid	Pressure (bar)	Temperature (°C)
1	BS1, BS2, BS3	H_2	No	150	100
2	BS4, BS5, BS6	H_2	Yes	150	100
3	BS7, BS8, BS9	Helium	Yes	150	100
/	BS10, BS11	Air	No	1	100

3. Results

3.1. Mineral compositions of the sandstones

The detrital mineralogy of all samples is dominated by quartz with 57.3% on average based on point counting results (Supplementary Material Table A1). Feldspar (K-feldspar and plagioclase) in all samples is the second most abundant detrital component and occurs almost exclusively as K-feldspar with 8.5% on average. The normalized amounts of quartz, feldspar, and rock fragments (shale, siltstone, sandstone rock fragments, chert, dolomitic ooids, limestone RF, quartzite, metamorphic, and plutonic rock fragments) display that the samples predominantly classify as subarkose, except for BS7 as lithic arkose (Fig. 2). Accessory minerals are muscovite, biotite, chlorite opaque minerals, tourmaline, zircon, and rutile. Clay mineral laminae, stained red by iron oxides and pore-lining illite can also be found in most of the samples. The most prominent authigenic constituents are syntaxial quartz and K-feldspar overgrowth cements, calcite, dolomite, anhydrite, barite, chlorite, and iron oxides. The latter two are either appearing as pore-lining or pore-filling. Illite, carbonates, and anhydrite all replace K-feldspar. Samples BS1, BS4, and BS8 contain a higher content of authigenic sulphates (mainly anhydrite and barite). Iron oxides are mostly present as pigmented to continuous hematite rims on detrital grains and intermixed with clay minerals in individual laminae. Carbonates occur either as dolomitic ooids or as pore-filling and syntaxial cements (calcite and dolomite). It is important to note that none of the samples contain any detectable pyrite based on the thin section analysis, which is consistent with findings from similar formation rocks [16,55].

Minerals that may react to hydrogen exposure include sulphates (e.g., anhydrite and gypsum), sulfides (e.g., pyrite), carbonates (e.g., calcite and dolomite), Fe^{3+}-bearing clay minerals (e.g., illite and chlorite), and iron oxides (e.g., hematite and goethite) [21]. Hence, the minerals identified through point counting were categorized into four key groups: clay minerals, carbonates, sulphates, and iron oxides (Fig. 3). Although the mineralogical composition of the samples varies due to different textures, the selected samples for each experimental condition contain representative amounts of reactive minerals, which are relatively comparable.

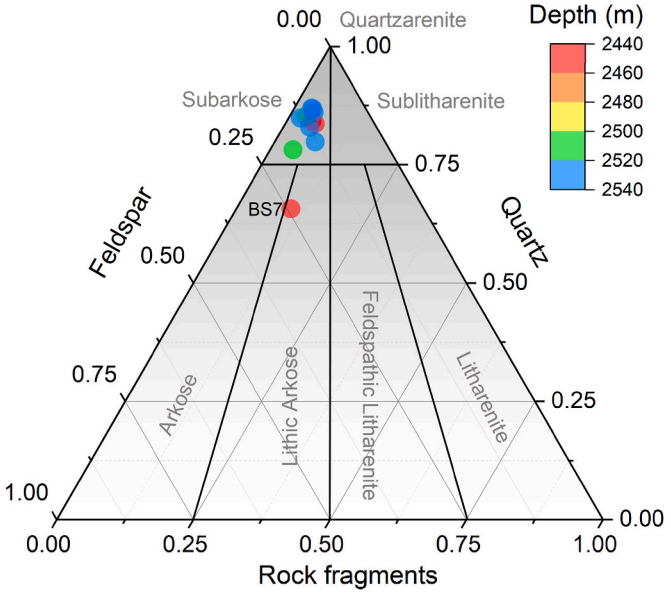

Fig. 2. Ternary quartz-feldspar-rock fragment classification diagram [56] of the studied Buntsandstein reservoir rocks.

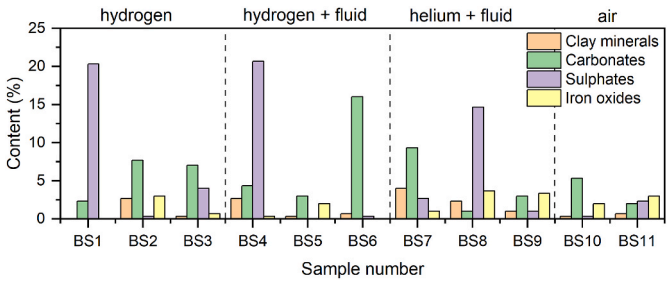

Fig. 3. Mineral contents of samples before the experiment that may react with hydrogen, along with the experimental conditions of the different groups. Mineral compositions are derived from point-counting of thin sections.

3.2. Pressure variations in batch reactors

The entire pressure variations in the hydrogen reactors were recorded throughout the experiments (Fig. 4). The hydrogen reactors 1 and 2 were sufficiently gas-tight, and the hydrogen pressure in reactor 1 was nearly unchanged over the entire four weeks. In the hydrogen + fluid saturated reactor 2, the hydrogen pressure initially built up to 154 bar gradually decreased at the beginning, and eventually stabilized at 147 bar after approximately 5 days. It is important to note that the total hydrogen volume injected into reactor 2 is much smaller than in reactor 1 due to the volume occupied by the fluid in reactor 2 (saline fluid-saturated). Thus, pressure in reactor 2 will be more sensitive to gas molecule loss in comparison to the pressure in the large volume of reactor 1.

3.3. Petrophysical properties

An increase in porosity was observed for all samples after the batch experiments, particularly for samples under saline fluid-saturated conditions, i.e., hydrogen + fluid and helium + fluid (Table 2 and Fig. 5). Samples BS4 and BS8 show the largest increase in porosity with relative enhancements of 17.5% and 14.6%, respectively. Furthermore, samples subjected to dry conditions exhibit comparable levels of porosity increase within approximately 5% of their initial values, in both oxidation (air) and reducting (hydrogen) environments.

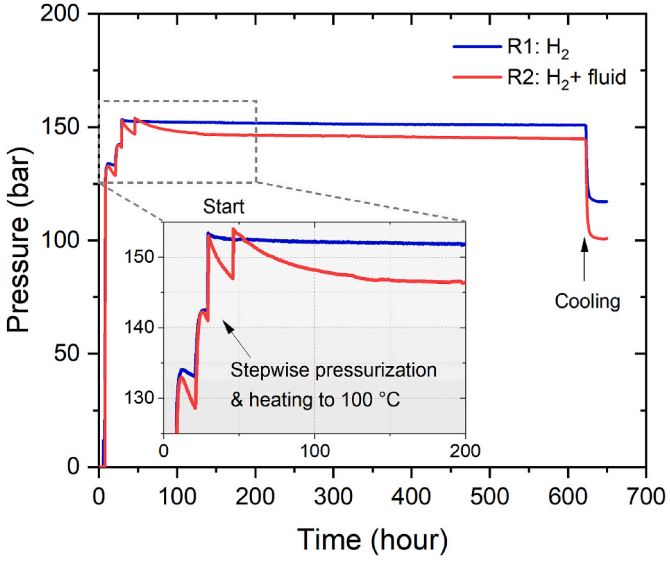

Fig. 4. Pressure records for hydrogen batch reactors over four weeks indicate that the pressure was initially increased to approximately 130 bar at room temperature. Subsequently, it was further adjusted to 150 bar under elevated temperature of 100 °C.

In contrast, changes in permeability are not consistent in the samples (Table 2 and Fig. 6). Most samples have a negligible permeability change within 5% relative to their initial permeabilities. Samples BS4 and BS9 under the aqueous conditions show slightly higher permeability changes with increases of 10.6% and 12.6%, respectively. However, for low permeability sample BS6, a permeability reduction from 0.47 mD to 0.38 mD with a relative decrease of 19% was obtained. Permeability changes are all within the same order of magnitude and changes are minor.

3.4. Magnetic susceptibility

All samples exhibit low mass-normalized magnetic susceptibility values, ranging between 10^{-8} to 10^{-7} m^3/kg (Table 2 and Fig. 7). These findings suggest an absence of ferrimagnetic minerals, such as magnetite or pyrrhotite in the initial rock samples. The changes in mass-normalized magnetic susceptibility of samples before and after the batch experiments are negligible, suggesting the absence of magnetic mineral transformations under all conditions.

3.5. Fluid element concentration

Fluid element concentration analysis shows that the major elements Na, Ca, K, Mg, Sr, and Si, are present on a scale of mg/L (ppm) (Fig. 8a). Additionally, the trace elements Li, B, Al, Cr, Mn, Fe, Cu, Zn, As, Rb, Sb, Ba, Pb are shown on a scale of μg/L (ppb) (Fig. 8b) (Supplementary Material Table A2). It is observed that the concentration of all elements, except for the trace elements Al and Fe, increased after the batch experiments conducted in both helium and hydrogen aqueous environments. The increased element concentration implies additional mineral dissolution in the synthetic fluid during the experiments. Aluminium was not detectable in the fluids after the batch experiments possibly due to the formation of other minerals, e.g., hydrobasaluminite [57]. Fe concentration under helium aqueous conditions decreased but increased slightly under the hydrogen brine environment. Additionally, the concentration of most elements in reactor 3 (helium) is slightly higher than those in reactor 2 (hydrogen), except for Cr, Fe, and Ba. The pH values of the initial fluid and the effluent in reactors 2 and 3 are about 7 (neutral) measured with a pH indicator strip.

3.6. Petrographic analysis

The frequently occurring pore-filling anhydrite, carbonate cement, and occasionally occurring carbonate ooids are of particular interest in this study. Because they are potential reactive minerals and some of them are directly connected with the open pores, where potential redox or decomposition reactions may happen. Sulphates (mainly anhydrite with the rare occurrence of gypsum and barite) were commonly found in initial samples (Fig. 9). Anhydrite appears with a high birefringence with bright interference colors under crossed-polarized light (XPL). Anhydrite fills the spaces between sand grains, appearing as a pore-filling cement. Dissolution features of anhydrite were detected by the comparison between the initial and altered textures before and after the batch experiments, where alteration created voids and vugs within the anhydrite only in reactors 2 and 3 under the fluid-saturated conditions (Fig. 9d and f). The dissolution of anhydrite created secondary porosity mostly along the cleavage planes, thus enhancing the total porosity of the sandstone and the connectivity between pores, which are consistent with the helium porosity measurements (Fig. 5). Additionally, samples BS1, BS4, and BS8 contain the largest amount of sulphates (Fig. 3), and the largest increase in porosity after batch experiments also occurred in samples BS4 and BS8 under wet conditions, implying a significant contribution from anhydrite dissolution. The dissolution features were found in both gas-fluid-saturated environments in reactors 2 and 3. Under dry conditions, e.g., hydrogen in reactor 1, there are no detectable changes in the anhydrite, barite, and gypsum mineral features, e.g.,

Table 2
Porosity, permeability, and mass normalized magnetic susceptibility of samples before and after batch experiments.

Samples	Porosity (%)		Permeability (mD)		Mass normalized magnetic susceptibility (m^3/kg)		Conditions
	Before	After	Before	After	Before	After	
BS1	6.44	6.66	49.90	48.69	6.92E-09	5.59E-09	H_2
BS2	15.08	15.61	367.00	353.74	4.51E-08	4.53E-08	H_2
BS3	23.12	23.73	1874.69	1768.68	1.13E-07	1.09E-07	H_2
BS4	8.48	9.96	40.10	44.37	4.42E-08	4.38E-08	H_2 + fluid
BS5	16.62	17.42	1512.07	1533.09	1.39E-08	1.35E-08	H_2 + fluid
BS6	7.71	8.33	0.47	0.38	4.80E-08	4.61E-08	H_2 + fluid
BS7	13.68	14.59	11.00	10.51	1.74E-07	1.73E-07	He + fluid
BS8	8.73	10.00	24.19	23.83	1.46E-07	1.46E-07	He + fluid
BS9	18.05	18.59	713.47	803.53	7.04E-08	6.91E-08	He + fluid
BS10	14.72	15.37	27.95	29.13	5.21E-08	4.98E-08	Air
BS11	16.29	16.37	167.23	164.18	6.49E-08	6.52E-08	Air

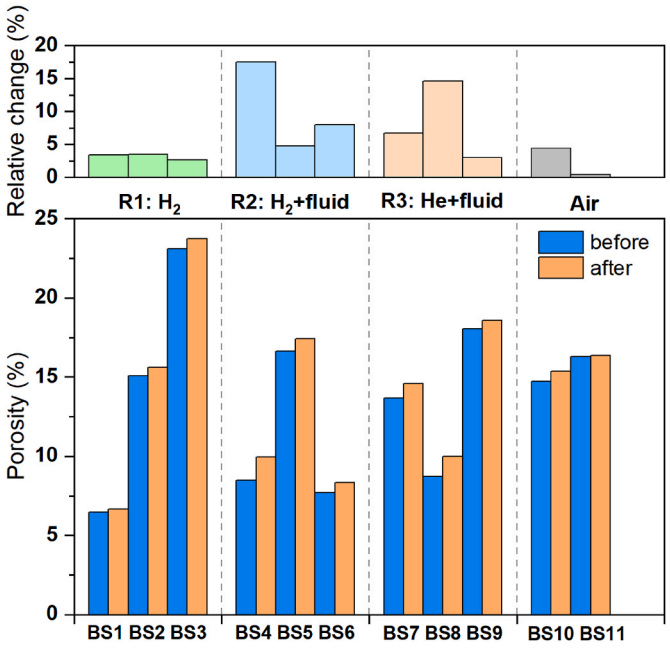

Fig. 5. Comparison of porosity before and after the batch experiments (Table 2), including plots of relative porosity changes compared to their initial values, as (after - before)/before.

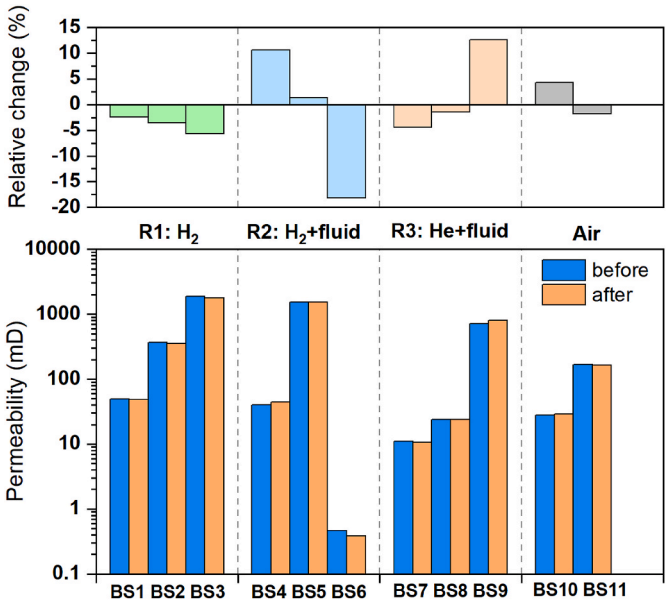

Fig. 6. Comparison of permeability before and after the batch experiments (Table 2), including plots of relative permeability changes compared to their initial values, as (after - before)/before.

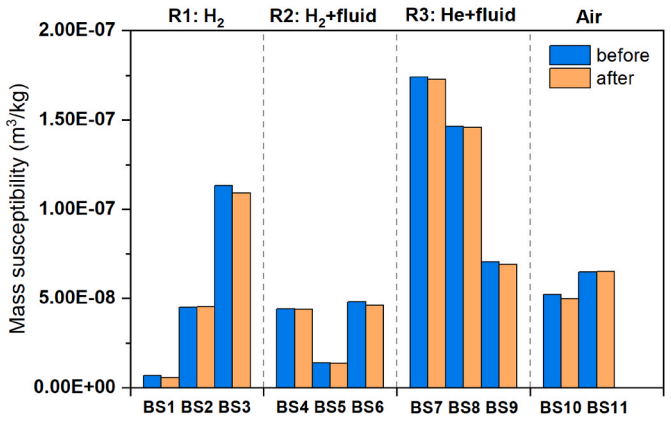

Fig. 7. Comparison of mass-normalized magnetic susceptibility of samples before and after the batch experiments (Table 2).

dehydration and hydration.

There is no detectable evidence of calcite reactions, such as dissolution and precipitation, in the thin sections (Fig. 10), under either dry (hydrogen) or hydrogen/helium-brine saturated conditions. The comparison of calcite before and after batch experiments reveals that no voids and secondary porosity were generated in the calcite crystals to enhance porosity (Fig. 10b and h). As dolomitic ooids appear partially dissolved in samples both before (BS1 Fig. 10e) and after the experiments (BS4 Fig. 10f), it is unlikely that they are the main contributor to Ca and Mg in solution following the batch experiments under the hydrogen-brine saturated condition. The dissolution features of dolomitic ooids likely existed in the samples originally. Nevertheless, we did not find sufficient one-to-one comparison between the initial materials and the altered samples under the hydrogen-brine condition, which may suggest that hydrogen potentially facilitated calcite dissolution.

Finally, the petrographic analyses of the altered samples revealed no significant changes in the mineral morphology of quartz, iron oxide rims, and crystals (e.g., hematite and goethite), and both pore-lining and pore-filling clays (Fig. 10).

4. Discussion

The reactivity of pure minerals, including sulphates, sulfides, iron oxides, and carbonates, with hydrogen under various conditions

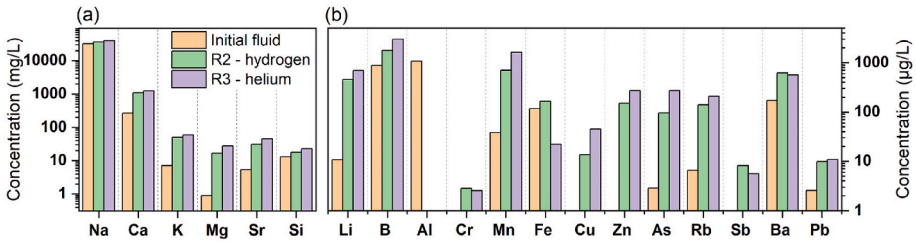

Fig. 8. Comparison of fluid element concentrations between the initial synthetic fluid and the fluids used to saturate and alter the samples under pure hydrogen + fluid (samples BS4, BS5, and S6) and pure helium + fluid conditions (samples BS7, BS8, and BS9), respectively. a) Major element concentration in mg/L (ppm), and b) trace element concentration in µg/L (ppb).

(temperature, pressure, and the presence or absence of water) has been extensively documented in previous geochemistry studies [21,24–26,28,29,31,32,37]. In this discussion, we evaluate whether hydrogen reactions occur in our reservoir sandstones under dry or fluid-saturated conditions by comparing hydrogen experiments with control experiments using helium and air (Fig. 1b). Although pyrite is not detected in our samples based on thin section analysis, we explore its potential trace amounts and effects for a comprehensive discussion.

4.1. Hydrogen reaction with solid phases

Carbonates, iron oxides, and pyrite can react with hydrogen under dry conditions. For instance, reactions of carbonates e.g., calcite, dolomite, and siderite with hydrogen can occur directly from a carbonate surface-gas reaction at primarily temperature-dependent conditions such as 500 °C and above [28,29].

$$CaCO_3 + 4H_2 = CaO + CH_4 + 2H_2O \quad (2)$$

$$CaCO_3 + 4H_2 = Ca(OH)_2 + CH_4 + H_2O \quad (3)$$

Hematite reduction in a pure hydrogen environment can occur at temperatures as low as 200 °C, with an increased reaction kinetics by raising hydrogen partial pressure from 30 bar to 80 bar [27]:

$$3Fe_2O_3 + H_2 = 2Fe_3O_4 + H_2O \quad (4)$$

Previous investigation on Fe(III)-bearing clays indicated the structural Fe(III) in the clays can be reduced by the adsorption of hydrogen gas even at 90–120 °C [34]. Furthermore, pyrite reduction by hydrogen was also observed at a range of temperatures between 250 °C and 700 °C with a pressure of up to 42.4 bar [24,31].

$$FeS_2 + (1-x)H_2 = FeS_{1+x} + (1-x)H_2S,\ 0 < x < 0.125 \quad (5)$$

Therefore, if any of the above reactions occur, a reduction of pressure in a closed system should be detectable. In our results, hydrogen pressure in reactor 1 was unchanged at 100 °C over four weeks (Fig. 4). Magnetic susceptibility measurements indicate that no magnetic minerals, such as magnetite [53] and pyrrhotite [54] were formed after the alteration under both reducing (pure hydrogen) and oxidizing (air) conditions (Fig. 7). This suggests that the reduction of hematite and/or pyrite did not occur. Furthermore, the dry experiments revealed no detectable changes in the mineral phases, including calcite, iron oxides, and anhydrite (Figs. 9 and 10).

However, a more recent autoclave experiment with pure minerals (fine powders at µm-nm scales) and dry hydrogen revealed that hematite and pyrite can oxidize significant amounts of hydrogen at 120 °C and 200 bar of hydrogen partial pressure [33]. Nevertheless, our results indicate that potential reactive minerals in natural sandstones are unlikely to react with hydrogen at temperatures up to 100 °C. The morphology and distribution of natural minerals, such as pyrite and hematite, in sandstones likely result in a very small effective surface area and limited contact interface with hydrogen. In the studied sandstone samples, hematite is particularly found at the edges of detrital grains and encased within pore-filling cements (Fig. 9a–c, Fig. 10a and b), which impacts its reactivity with fluids occupying the pore spaces. Most of them are mixtures with clays, further limiting potential reactions even under reactive pressure and temperature conditions. Results derived from pure particle mineral experiments [33] may overestimate the reaction kinetics if applied to natural rocks. Consequently, the mentioned hydrogen-mineral reactions, Eqs. (2)–(5), are primarily temperature-dependent and unlikely to occur under our simulated reservoir conditions (i.e., dry at 100 °C and 150 bar for four weeks).

4.2. Hydrogen reaction in aqueous environments

4.2.1. Carbonates

To date, research on hydrogen reactivity with rocks in aqueous environments has yielded disparities, particularly for reactions between hydrogen and carbonates. Most geochemical modeling work indicated that hydrogen dissociation in water facilitates carbonate dissolution and vice versa, with a by-product of methane, as shown below [21,35,36,43].

$$CO_3^{2-} + 4H_2 + 2H^+ = CH_4 + 3H_2O \quad (6)$$

Therefore, hydrogen loss and methane generation in carbonates and calcite-bearing rocks were always predicted in modeling, and the subsequent suggestion was targeting calcite-free rocks for hydrogen long-term storage [35,36]. Geochemical batch experiments revealed no facilitated calcite dissolution in a hydrogen-brine environment by analyzing fluid element concentration compared with blank tests [43,47]. Calcite dissolution exclusively induced by a hydrogen-brine treatment was observed in a claystone alteration experiment conducted over 30 days at room temperature [40]. Additionally, Al-Yaseri et al. [41] and Al-Yaseri et al. [42] reported some inconclusive results, indicating that carbonate expansion occurred under the hydrogen-brine condition at 75 °C and 48 bar over 75 days, leading to a porosity reduction of up to 50% [41]. Still, current experimental data and geochemical models do not align, necessitating further research to achieve consistency [43].

Based on our results, the increased concentrations of Ca and Mg may be correlated with carbonate dissolution (e.g., calcite and dolomite) (Fig. 8). However, there is no comparable evidence from petrographic analysis indicating that dissociated hydrogen facilitates the dissolution of calcite or dolomite (Fig. 10). Comparing with blank results in the helium-brine environment, hydrogen did not enhance carbonate solubility, causing more dissolved elements (Fig. 8). Therefore, we suggest that carbonate dissolution and the associated hydrogen loss (as described in Eq. (6)) are unlikely to be a significant reaction in sandstone rocks under our simulated conditions over four weeks. Therefore, we reconfirm the concern raised by Gelencsér et al. [43] that the modeling of calcite-hydrogen-brine reaction based on PHREEQC significantly overestimates the reaction kinetics. Future research on gas composition analysis, such as gas chromatography could provide definitive evidence of methane formation.

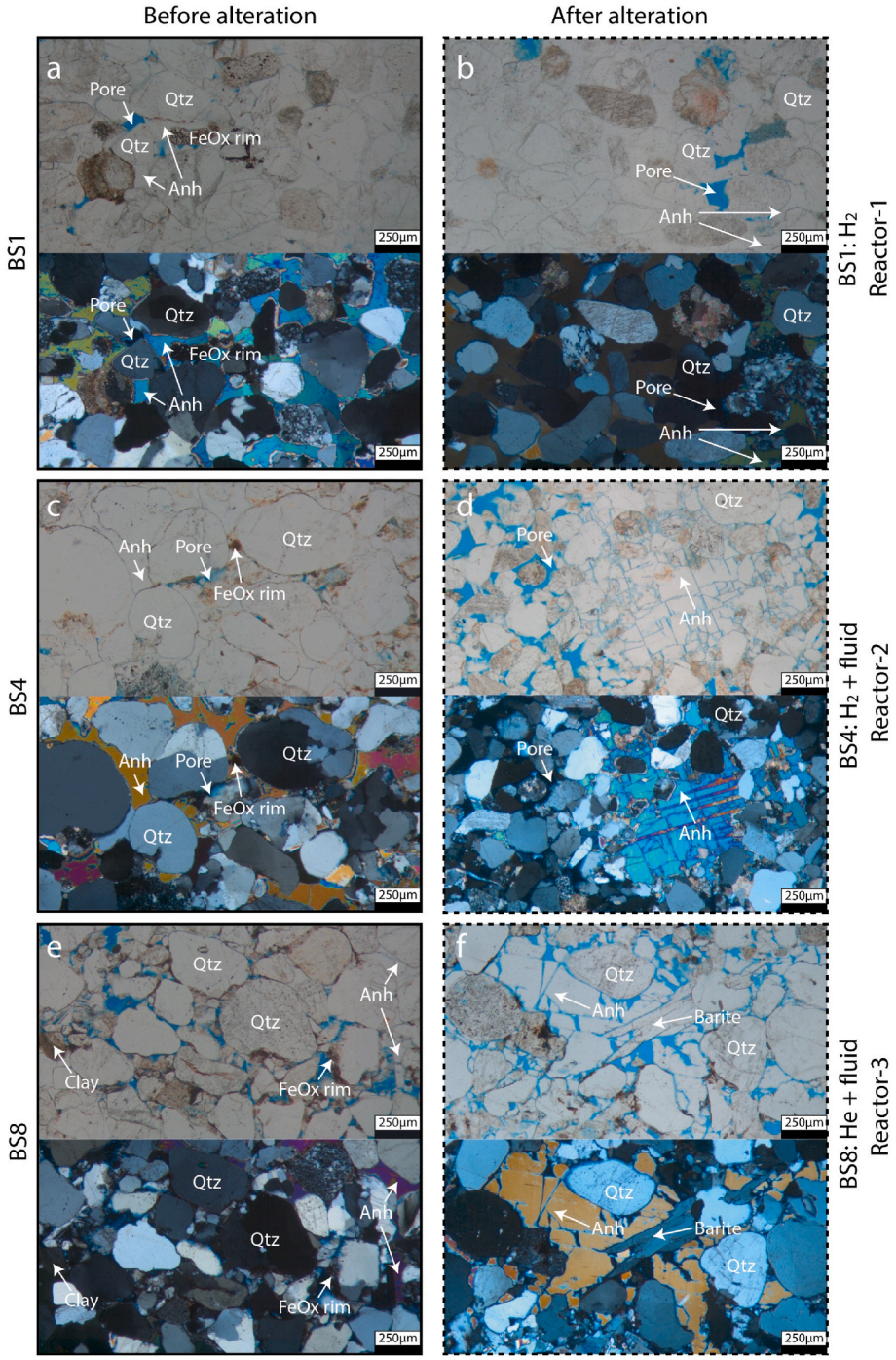

Fig. 9. Thin section images of the initial materials a) BS1, c) BS4, and e) BS8, and the corresponding altered samples b) BS1, d) BS4, and f) BS8, under an optical microscope with plane-polarized light (PPL) and crossed-polarized light (XPL). Blue areas indicate open pores. Anhydrite dissolution and alteration are found under both d) hydrogen + fluid and f) helium + fluid conditions but not under the dry hydrogen environment b). Barite in a needle shape is also observed in f) sample BS8, indicating barite dissolution. (For interpretation of the references to color in this figure legend, the reader is referred to the Web version of this article.)

4.2.2. Sulphates

For sulphate reactions, thin section analysis of the batch experiments revealed that anhydrite dissolution was the predominant reaction, leading to the generation of secondary porosity (Fig. 9). Consequently, samples BS4 and BS8, which contain the highest amounts of sulphates (see Fig. 3), yielded the greatest increase in porosity with 17.5% and 14.6%, respectively (Fig. 5), compared to other samples with lower sulphate content under the same condition. This confirms that anhydrite dissolution mainly contributes to porosity changes. Moreover, anhydrite dissolution also contributes to the increase in Ca concentration in the fluids after the batch experiments (Fig. 8). Nevertheless, sulphate dissolution includes thermodynamic non-reductive dissolution (Eq. (7)) and reductive dissolution (Eq. (8)) [25,58],

$$MSO_4 = M^{2+} + SO_4^{2-} \tag{7}$$

$$SO_4^{2-} + 4H_2 + 2H^+ = H_2S + 4H_2O \tag{8}$$

where, M refers to metal ions, e.g., Ca (anhydrite), Ba (barite), and Sr (celestite), which are all contained in our samples based on the fluid

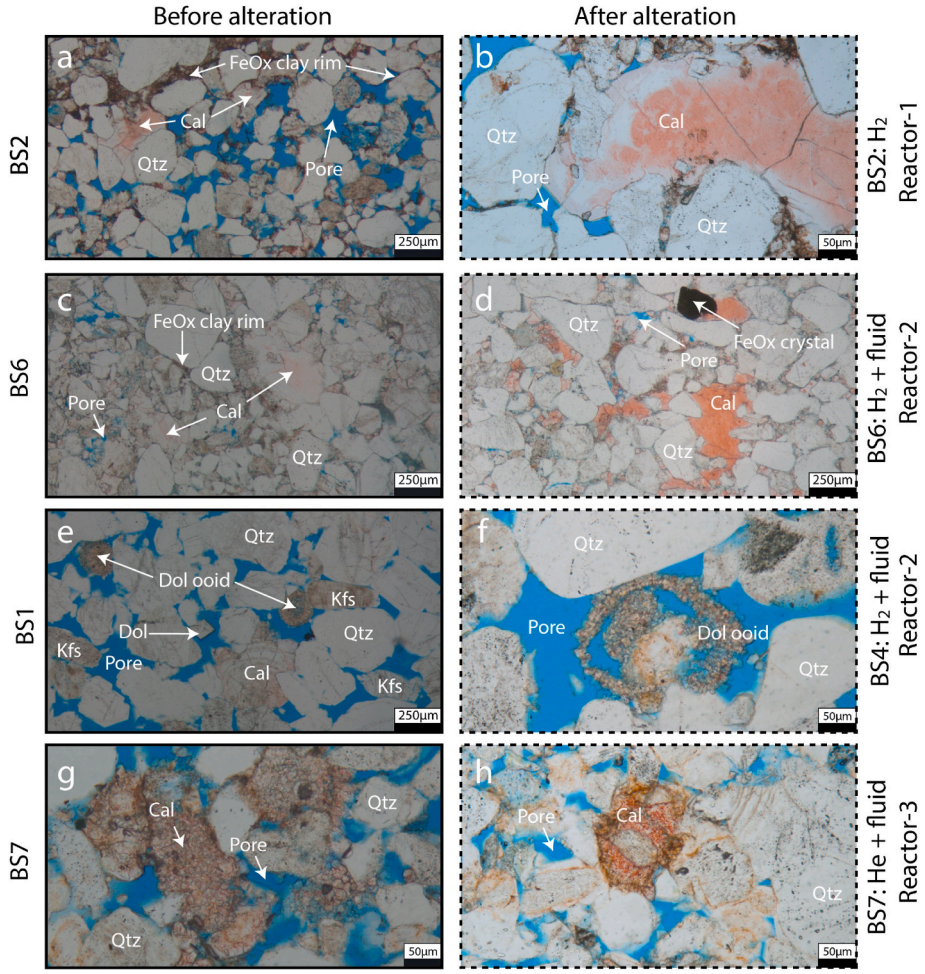

Fig. 10. Thin section images of representative initial sandstones a), c), e), and g), and the corresponding altered samples b), d), f), and h) under an optical microscope with plane-polarized light (PPL), where calcite does not show visible shape changes under the conditions of pure hydrogen, and helium + fluid, while some features of dissolution of dolomitic ooids were found in both the initial and the altered samples in e) and f). Iron oxide clay rims and crystals are also detected in e.g., a) and d), respectively.

element concentration (Fig. 8) and thin section analyses (Fig. 9). In the non-reductive dissolution, the concentration of M in the fluid is controlled by its dissolution kinetics and solubility. In contrast, sulphate reduction initiation requires H_2S as the catalyst for the reactive intermediates [25,39]. This implies that if sulphate reduction occurs in an H_2S-rich environment (e.g., produced by pyrite reduction), the process would be self-sustaining. In this case, the reduction of sulphate may indirectly further increase M concentration due to the dissolution of anhydrite driven by the removal of sulphate ions. Whether sulphate reduction (Eq. (8)) occurred in our experiments could not be confirmed except by measuring the presence and amounts of H_2S in the gas composition. While there is no substantial difference in element (M) concentrations between the hydrogen-brine and helium-brine environments (Fig. 8), this suggests limited or no sulphate reduction reactions (Eq. (8)) in the hydrogen environment. The alteration of anhydrite was primarily due to non-reductive dissolution (Eq. (7)).

4.2.3. Sulfides

The magnetic susceptibility results showed that no ferrimagnetic minerals were formed under any conditions (Fig. 7), indicating that the reduction of hematite to magnetite and pyrite to pyrrhotite did not occur. However, pyrite is thermodynamically unstable in the presence of hydrogen, leading to potentially significant hydrogen-induced redox reactions (Eq. (5)) even at low temperatures, such as between 90 and 250 °C, particularly in calcite buffered solutions with hydrogen partial pressures up to 30 bar [37,38]. Additionally, pyrite rapidly transforms into pyrrhotite at temperatures above 90 °C and hydrogen partial pressure exceeding 10 bar [38]. This reaction is further accelerated under alkaline conditions, such as those found in calcite solutions. However, in our experiments, pyrite was not observed in the thin section images (Figs. 9 and 10). The possible trace amounts of pyrite that reacted with hydrogen during the experiments are expected to have a negligible effect on the rock properties due to their minimal quantity. However, if pyrite is abundant (e.g., >1%) in calcite-bearing sandstones, the redox reaction of pyrite could pose a significant issue in hydrogen-brine environments [38]. This reaction may be facilitated by calcite dissolution forming an alkaline environment. This will need further investigation by analyzing the gas compositions during or after the experiments.

4.2.4. Iron oxides

The unchanged magnetic susceptibility indicated that iron oxides such as hematite and goethite remained stable under the experimental conditions (Fig. 7). Hematite (Fe_2O_3) has an extremely low solubility in water, especially under neutral pH conditions [59]. The variation in iron concentration before and after the batch experiments (Fig. 8) might be due to the reduction of dissolved Fe(III) to Fe(II) induced by hydrogen, resulting in more soluble Fe(II) [60] in the fluid without forming a solid magnetite phase or the dissolution of Fe(II) from carbonates or sulphates. However, this hypothesis is based on weak evidence and requires

further verification through additional batch experiments with pure hematite [27] or rock containing significant amounts of hematite. Overall, the solid iron oxides remained unchanged under our experimental conditions.

4.2.5. Fluid element concentration

Changes in the major element composition (Fig. 8a) reflect the primary dissolution reactions. Trace elements (less than 1 ppm Fig. 8b) are likely by-products of these major mineral dissolution processes or originate from minor mineral phases, which are too small to be observed in thin sections (Figs. 9 and 10). Another potential mechanism is the occurrence of mineral surface reactions in response to disequilibrium conditions within the fluid. Trace elements such as Li and Rb are likely dissolved from phyllosilicates, while Mn, Cu, Zn, As, and Pb can be desorbed due to redox reactions at the surfaces of iron oxide minerals. These trace elements are unlikely to affect rock performance. Consequently, we will not further discuss them, except aluminum (Al), which became undetectable after batch experiments.

The increased levels of Ca, Sr, and Ba suggest the dissolution of sulphates, primarily anhydrite with the occurrence of barite, which is consistent with the thin section analysis (Fig. 9). The elevated concentrations of Na and K are likely attributed to the dissolution of feldspar (K-feldspar and plagioclase), but the slight increase in Si concentration and low Al concentration indicate that feldspar dissolution is not significant. Additionally, dissolved Mg may be associated with the dissolution of dolomite. However, the comparison of the element concentration in both reactors indicates that hydrogen does not appear to facilitate further mineral dissolution in the fluid. The increase in element concentrations is related to the non-equilibrium of the synthetic fluid chemistry. Interestingly, we observed that the Al concentration (initially 1064 μg/L) became undetectable (<0.1 μg/L) in the fluid after batch experiments (Fig. 8). This significant reduction may be linked to mineral precipitation. In an environment with a high concentration of sulphate ions (SO_4^{2-}), dissolved aluminum precipitates at low pH (~4.0), forming an amorphous, globular hydroxysulphate precipitate with a composition corresponding to hydrobasaluminite [57,61].

$$4Al^{3+} + SO_4^{2-} + 14H_2O \leftrightarrow Al_4(SO_4)(OH)_{10} \bullet 4H_2O + 10H^+ \quad (9)$$

Sulphate dissolution was a major reaction in the experiments, resulting in significantly higher sulphate concentrations (i.e., 554 mg/L in the initial fluid, see Section 2.4). Hydrobasaluminite precipitation is suggested to occur in our experiments. However, a low pH is typically required for hydrobasaluminite precipitation, which may also result from artificial effects due to the addition of 1% HNO_3 in the solution during fluid sample preparation for ICP-OES analysis. An alternative mineral formation is aluminum hydroxides, which can form from saturated fluids at a neutral pH, as observed in our experiments. In summary, by comparing element concentrations in hydrogen and helium environments, no hydrogen-facilitated reactions were observed.

4.2.6. Hydrogen dissolution

Hydrogen pressure in the dry condition (reactor 1) was extremely stable over four weeks, but hydrogen pressure reduced as soon as the pressure was built up and converged within the first 5 days in the brine-filled reactor 2 (Fig. 4). This behavior is likely related to hydrogen dissolution in the saline fluid, where the extent of pressure reduction is correlated with hydrogen solubility and the volume ratio between the gas and the liquid phases. Reactor 2 was nearly filled with fluid, leaving only a small volume at the very top of the reactor and the capillary volume for the compressed hydrogen, V_H, which is approximately 60 mL. The net volume of the synthetic fluid (V_L), after accounting for the volume occupied by the solid rock, is approximately 131 mL. Based on the ideal gas law,

$$PV = nRT \quad (10)$$

where P (Pa) is the gas pressure, V (m^3) is the volume, T (K) is temperature, n (mol) is the number of moles of the gas and R ($m^3 \cdot Pa \cdot K^{-1} \cdot mol^{-1}$) is the universal gas constant. We calculated, that a pressure drop from 154 bar to 147 bar at a constant temperature of 100 °C (Fig. 4 and section 3.2), results in a a reduction of hydrogen molarity in V_H from 0.29782 mol to 0.28428 mol, corresponding to a decrease of $1.354x10^{-2}$ mol of hydrogen.

Based on the experimentally-varified model by Ref. [15], hydrogen solubility in an 8% NaCl solution (1.37 mol/L) at 100 °C and 150 bar is approximately $1.4638x10^{-3}$ in mole fraction, which converts to $8.0623x10^{-2}$ mol/L. Therefore, the theoretically dissolved hydrogen in our synthetic fluid volume (V_L = 131 mL) is about $1.056x10^{-2}$ mol, which is slightly less than the theoretical hydrogen loss ($1.354x10^{-2}$ mol) calculated based on Eq. (10) and the pressure drop shown in Fig. 4. Although the measured gas volume in the system lacks precision, the derived theoretical hydrogen loss is of the same order of magnitude as the dissolved hydrogen. This suggests that the pressure reduction is primarily due to the hydrogen dissolution in our experiments.

4.3. Effects of hydrogen reactivity on rock properties

There is a notable lack of research on changes in rock petrophysical properties, such as porosity and permeability, induced by hydrogen exposure. An exception is the study of Flesch et al. [16], which observed an average increase in porosity from 20% to 24%, while permeability showed only minor changes in Triassic drill core sandstones from northwest Germany. Our observations of porosity and permeability changes under wet conditions (Figs. 5 and 6) align well with the results of Flesch et al. [16]. The increase in porosity mainly results from anhydrite dissolution, which has a minimal impact on permeability changes. The most significant relative decrease in permeability was observed in a low-permeability sample (BS6) with a reduction from 0.47 mD to 0.38 mD (Table 2), likely due to the precipitation of secondary mineral phases in narrower pore throats. These changes are related to fluid-rock interactions caused by the non-equilibrium between rock minerals and the synthetic fluid, as evidenced by comparisons under helium and hydrogen environments (Figs. 5–7). We further demonstrated that hydrogen does not facilitate any geochemical reactions, including carbonates (e.g., calcite) and sulphates (e.g., anhydrite), which are often presumed to occur under exposure to hydrogen in aquous environments at temperatures even below 100 °C [16,22,35,41]. Additionally, under dry conditions, we confirmed that hydrogen does not react directly with minerals under our simulated pressure and temperature conditions.

Our comprehensive experimental findings challenge the prevailing notion regarding the reactivity of carbonates and sulphates with hydrogen in reservoir environments, where temperatures are typically below 100 °C [16,22,35,36,40,41]. It is essential to differentiate between geochemical reactions caused by the non-equilibrium of fluid chemistry and those facilated by hydrogen. Notably, many reactions observed in batch experiments are due to fluid-rock interactions rather than direct effects of hydrogen. This distinction must be carefully considered in future experimental designs and interpretations.

4.4. Implications for underground hydrogen storage in porous rocks

The simulated dry and hydrogen-brine saturated conditions represent distinct regions within reservoirs, such as the dry-out zone near the wellbore, partially-saturated zones with residual brine, and fully-saturated deep formations (Fig. 11). Our findings indicate that abiotic geochemical reactions do not occur in the dry-out zone near the wellbore or in some dry reservoirs. This is advantageous, as permeability near the wellbore has the greatest effect on reservoir injectivity. In the gas-brine two-phase flow zone, potential reactions will highly depend on the distribution of residual brine relative to mineral surfaces. Although

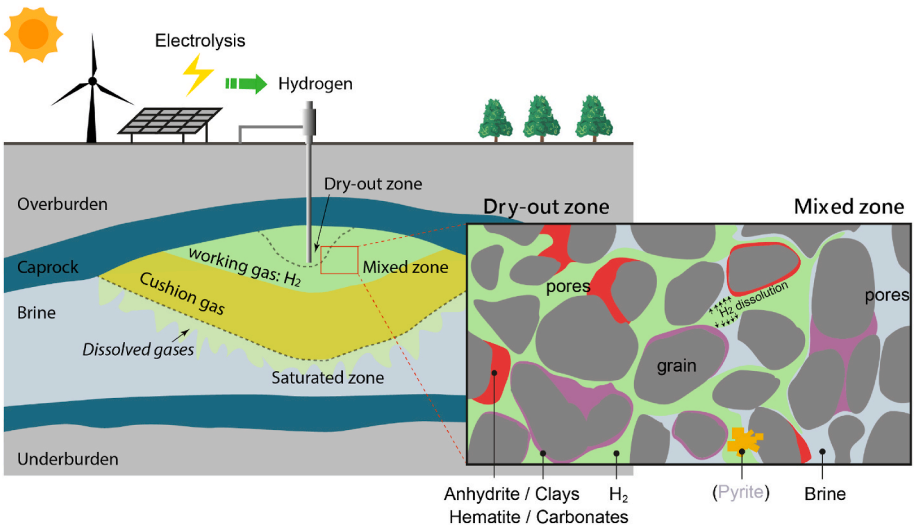

Fig. 11. Schematic sketch of underground hydrogen storage in a porous reservoir, featuring a dry-out zone near the wellbore, a mixed zone containing residual brine and gases, and a saturated zone below the cushion gas. The zoomed-in grain-scale profile illustrates gas and fluid distributions relative to different minerals in the dry-out and mixed zones, where hydrogen could dissolve into the residual brine potentially reacting with minerals.

hydrogen reactions may occur over long-term periods (spanning decades to hundreds of years as noticed by Bo et al. [35] and Zeng et al. [36]), they are unlikely to affect reservoir performance significantly due to the increased flow pathways further away from the wellbore. In the fully saturated zone, where cushion gases (e.g., CH_4, N_2, or CO_2) are in direct contact, effectively isolating the working gas hydrogen above, as shown in Fig. 11 [62]. Consequently, the abiotic geochemical reactivity of hydrogen and its effects on reservoir performance are not major concerns in the studied reservoir sandstones. The risk of abiotic hydrogen loss and a decline in reservoir integrity is therefore expected minimal.

4.5. Limitations of current methods

Previous studies in pure mineral chemistry have established that sulfide, sulphates, carbonates, and iron oxides are reactive with hydrogen under specific elevated temperature and pressure conditions, with and/or without the presence of water [25,27–29,32,33,37,38]. However, experimental results on hydrogen alteration in natural reservoir rocks show significant disparities. Our findings support the feasibility of storing hydrogen in sandstone reservoirs containing sulphates, iron oxides, and carbonates, as no significant reactions were observed that could adversely impact reservoir performance. This indicates that most hydrogen-reactive minerals (sulphates, carbonates, and iron oxides) require much higher temperatures to react (see section 1 Introduction) than those typical of reservoir conditions.

It is important to note that our samples did not contain detectable amounts of pyrite, a mineral known to be more reactive with hydrogen [e.g., 24, 32, 37, 38] under both dry and wet conditions at relatively low temperatures (e.g., 90 °C as noted by Truche et al. [37]). Pyrite can react with hydrogen to form H_2S, which not only catalyzes sulphate reduction reactions [25,39], but also acidifies fluids and increases ionic strength through dissolution. This, in turn, may enhance fluid-rock interactions, destabilize clay minerals, and affect carbonate stability. Consequently, our experimental results may not fully apply to reservoirs containing pyrite. Further studies should focus on pyrite-bearing sandstones to better understand the complexities of hydrogen reactivity in these systems.

Our experiments were conducted over a duration of four weeks, which may not capture reactions with extremely low reaction rates. However, reaction kinetics are typically more pronounced in the early stages of closed batch experiments, where conditions are far from equilibrium. A four-week time frame aligns with durations commonly used in current research, ranging from a few days to several months [16,41–43,46], and likely provides a reasonable representation of the prevailing reactivity. Additionally, whether trace amounts of H_2S are formed due to pyrite or sulphate (e.g., anhydrite) reduction, and CH_4 due to carbonate reactions with hydrogen during the experiments, warrants further investigation. Gas chromatography (GC) analysis would provide additional insights and strengthen confidence in the long-term predictions of reservoir behavior under hydrogen storage conditions.

5. Conclusions

Our study suggests that hydrogen exhibits minimal reactivity with reservoir rocks, specifically pyrite-free Buntsandstein sandstone from a gas field, under simulated reservoir conditions of 100 °C and 150 bar hydrogen partial pressure over four weeks. Potential mineral transformations, such as the conversion of hematite to magnetite/iron, did not occur under these simulated conditions. Furthermore, major hydrogen-reactive minerals like sulphates, carbonates, and iron oxides, are unlikely to be affected by hydrogen under these reservoir conditions, except for dissolution and precipitation due to chemical disequilibrium. No significant changes in reservoir performance including permeability and porosity, were observed due to hydrogen exposure. Reactions involving these minerals typically require much higher temperatures and greater effective surface area to initiate. Although often described in modeling studies, the alteration of carbonates was not observed during our experiments. In summary, abiotic geochemical reactions with reservoir rocks, and their effects on hydrogen loss and reservoir performance degradation, do not pose a risk during underground hydrogen storage in this section of the studied reservoir lithology. However, our results do not provide an answer regarding the suitability of samples containing slightly higher amounts of pyrite (>1%) for hydrogen storage, due to the absence of pyrite in the studied samples. Additionally, because geochemical reactions are sensitive to temperature, further studies should investigate bulk samples at higher temperatures and measure gas composition to enhance confidence in the findings.

CRediT authorship contribution statement

Chaojie Cheng: Writing – original draft, Methodology, Investigation, Formal analysis, Data curation, Conceptualization. **Benjamin Busch:** Writing – review & editing, Methodology, Investigation,

Conceptualization. **Agnes Kontny:** Writing – review & editing, Methodology, Investigation. **Christoph Hilgers:** Writing – review & editing, Supervision, Project administration, Funding acquisition, Conceptualization.

Declaration of competing interest

The authors declare that they have no known competing financial interests or personal relationships that could have appeared to influence the work reported in this paper.

Acknowledgement

This work is part of the SAMUH2 project supported by the German Federal Ministry of Economic Affairs and Climate Action (BMWK) under grant no. 03EI3051A. The authors wish to thank Kevin Altinger for manufacturing the batch reactors, Martin von Dollen for thin section preparation, Johanna Berckhan and Bruno Daniel Leite Mendes for the assistance with magnetic susceptibility measurements, Dr. Elisabeth Eiche for the measurements of fluid element concentration and insightful discussion, and Neptune Energy Holding Germany GmbH for provision of core material and permission to publish the results. The first author also gratefully acknowledges the constructive discussion on hydrogen-hematite reaction experiments with Prof. Helge Stanjek and Nicolai Thüns (both RWTH Aachen). Open access funding enabled and organized by Projekt DEAL.

Appendix A. Supplementary data

Supplementary data to this article can be found online at https://doi.org/10.1016/j.ijhydene.2025.01.330.

References

[1] Carden P, Paterson L. Physical, chemical and energy aspects of underground hydrogen storage. Int J Hydrogen Energy 1979;4(6):559–69. https://doi.org/10.1016/0360-3199(79)90083-1.
[2] Zgonnik V. The occurrence and geoscience of natural hydrogen: a comprehensive review. Earth Sci Rev 2020;203:103140. https://doi.org/10.1016/j.earscirev.2020.103140.
[3] Prinzhofer A, Cissé CST, Diallo AB. Discovery of a large accumulation of natural hydrogen in Bourakebougou (Mali). Int J Hydrogen Energy 2018;43(42):19315–26. https://doi.org/10.1016/j.ijhydene.2018.08.193.
[4] Miocic J, Heinemann N, Edlmann K, et al. Underground hydrogen storage: a review. Geol Soc London, Special Pub 2023;528(1):88. https://doi.org/10.1144/SP528-2022-88. SP528-2022.
[5] Stone HB, Veldhuis I, Richardson RN. Underground hydrogen storage in the UK. Geol Soc London, Special Pub 2009;313(1):217–26. https://doi.org/10.1144/SP313.13.
[6] Heinemann N, Alcalde J, Miocic JM, et al. Enabling large-scale hydrogen storage in porous media–the scientific challenges. Energy Environ Sci 2021;14(2):853–64. https://doi.org/10.1039/D0EE03536J.
[7] Thaysen EM, McMahon S, Strobel GJ, et al. Estimating microbial growth and hydrogen consumption in hydrogen storage in porous media. Renew Sustain Energy Rev 2021;151:111481. https://doi.org/10.1016/j.rser.2021.111481.
[8] Strobel G, Wirth M, Hagemann B, et al. Utilization of microfluidics to investigate microbial activity in underground hydrogen storage. In: 2nd geoscience & engineering in energy transition conference. European Association of Geoscientists & Engineers; 2021. https://doi.org/10.3997/2214-4609.202121039.
[9] Dohrmann AB, Krüger M. Microbial H2 consumption by a formation fluid from a natural gas field at high-pressure conditions relevant for underground H2 storage. Environ Sci Technol 2023;57(2):1092–102. https://doi.org/10.1021/acs.est.2c07303.
[10] Khajooie S, Gaus G, Dohrmann AB, et al. Methanogenic conversion of hydrogen to methane in reservoir rocks: an experimental study of microbial activity in water-filled pore space. Int J Hydrogen Energy 2024;50:272–90. https://doi.org/10.1016/j.ijhydene.2023.07.065.
[11] Lysyy M, Liu N, Solstad CM, et al. Microfluidic hydrogen storage capacity and residual trapping during cyclic injections: implications for underground storage. Int J Hydrogen Energy 2023;48(80):31294–304. https://doi.org/10.1016/j.ijhydene.2023.04.253.
[12] Zhang Y, Bijeljic B, Gao Y, et al. Pore-scale observations of hydrogen trapping and migration in porous rock: demonstrating the effect of Ostwald Ripening. Geophys Res Lett 2023;50(7):e2022GL102383. https://doi.org/10.1029/2022GL102383.
[13] Iglauer S, Ali M, Keshavarz A. Hydrogen wettability of sandstone reservoirs: implications for hydrogen geo-storage. Geophys Res Lett 2021;48(3):e2020GL090814. https://doi.org/10.1029/2020GL090814.
[14] Liu N, Kovscek AR, Fernø M, et al. Pore-scale study of microbial hydrogen consumption and wettability alteration during underground hydrogen storage. Front Energy Res 2023;11. https://doi.org/10.3389/fenrg.2023.1124621. 1124621.
[15] Chabab S, Theveneau P, Coquelet C, et al. Measurements and predictive models of high-pressure H2 solubility in brine (H2O+ NaCl) for underground hydrogen storage application. Int J Hydrogen Energy 2020;45(56):32206–20. https://doi.org/10.1016/j.ijhydene.2020.08.192.
[16] Flesch S, Pudlo D, Albrecht D, et al. Hydrogen underground storage—petrographic and petrophysical variations in reservoir sandstones from laboratory experiments under simulated reservoir conditions. Int J Hydrogen Energy 2018;43(45):20822–35. https://doi.org/10.1016/j.ijhydene.2018.09.112.
[17] Aftab A, Hassanpouryouzband A, Xie Q, et al. Toward a fundamental understanding of geological hydrogen storage. Ind Eng Chem Res 2022. https://doi.org/10.1021/acs.iecr.1c04380.
[18] Haddad P, Ranchou-Peyruse M, Guignard M, et al. Geological storage of hydrogen in deep aquifers–an experimental multidisciplinary study. Energy Environ Sci 2022;15(8):3400–15. https://doi.org/10.1039/D2EE00765G.
[19] Hemme C, Van Berk W. Hydrogeochemical modeling to identify potential risks of underground hydrogen storage in depleted gas fields. Appl Sci 2018;8(11):2282. https://doi.org/10.3390/app8112282.
[20] Pan B, Yin X, Ju Y, et al. Underground hydrogen storage: influencing parameters and future outlook. Adv Colloid Interface Sci 2021;294:102473. https://doi.org/10.1016/j.cis.2021.102473.
[21] Zeng L, Sarmadivaleh M, Saeedi A, et al. Storage integrity during underground hydrogen storage in depleted gas reservoirs. Earth Sci Rev 2023:104625. https://doi.org/10.1016/j.earscirev.2023.104625.
[22] Braid H, Taylor K, Hough E, et al. Hydrogen-induced mineral alteration: a review in the context of underground hydrogen storage (UHS) in saline aquifers. Earth Sci Rev 2024:104975. https://doi.org/10.1016/j.earscirev.2024.104975.
[23] Reitenbach V, Ganzer L, Albrecht D, et al. Influence of added hydrogen on underground gas storage: a review of key issues. Environ Earth Sci 2015;73(11):6927–37. https://doi.org/10.1007/s12665-015-4176-2.
[24] Lambert J, Simkovich G, Walker P. The kinetics and mechanism of the pyrite-to-pyrrhotite transformation. Metall Mater Trans B 1998;29:385–96. https://doi.org/10.1007/s11663-998-0115-x.
[25] Truche L, Berger G, Destrigneville C, et al. Experimental reduction of aqueous sulphate by hydrogen under hydrothermal conditions: implication for the nuclear waste storage. Geochem Cosmochim Acta 2009;73(16):4824–35. https://doi.org/10.1016/j.gca.2009.05.043.
[26] Jozwiak W, Kaczmarek E, Maniecki T, et al. Reduction behavior of iron oxides in hydrogen and carbon monoxide atmospheres. Appl Catal Gen 2007;326(1):17–27. https://doi.org/10.1016/j.apcata.2007.03.021.
[27] Thüns N, Krooss B, Zhang Q, et al. The effect of H2 pressure on the reduction kinetics of hematite at low temperatures. Int J Hydrogen Energy 2019;44(50):27615–25. https://doi.org/10.1016/j.ijhydene.2019.08.178.
[28] Giardini A, Salotti C, Lakner J. Synthesis of graphite and hydrocarbons by reaction between calcite and hydrogen. Science 1968;159(3812):317–9. https://doi.org/10.1126/science.159.3812.317.
[29] Giardini AA, Salotti CA. Kinetics and relations in the calcite-hydrogen reaction and relations in the dolomite-hy-drogen and siderite-hydrogen systems. Am Mineral: J Earth Planetary Mater 1969;54(7–8):1151–72.
[30] Henkel S, Pudlo D, Werner L, et al. Mineral reactions in the geological underground induced by H2 and CO2 injections. Energy Proc 2014;63:8026–35. https://doi.org/10.1016/j.egypro.2014.11.839.
[31] Wiltowski T, Hinckley C, Smith GV, et al. Kinetics and mechanisms of iron sulfide reductions in hydrogen and in carbon monoxide. J Solid State Chem 1987;71(1):95–102. https://doi.org/10.1016/0022-4596(87)90146-0.
[32] Ostertag-Henning C, Alperman T, Krüger M, et al. Transport of hydrogen in rocks considering abiotic chemical and microbial redox reactions: the H2_ReacT research projects. In: 2nd geoscience & engineering in energy transition conference. European Association of Geoscientists & Engineers; 2021. https://doi.org/10.3997/2214-4609.202121064.
[33] Alpermann T, Ostertag-Henning C. Abiotic redox reactions of H2 with iron-containing minerals under geologic storage conditions. In: EAGE/DGMK joint workshop on underground storage of hydrogen. European Association of Geoscientists & Engineers; 2019. https://doi.org/10.3997/2214-4609.201900263.
[34] Didier M, Leone L, Greneche J-M, et al. Adsorption of hydrogen gas and redox processes in clays. Environ Sci Technol 2012;46(6):3574–9. https://doi.org/10.1021/es204583h.
[35] Bo Z, Zeng L, Chen Y, et al. Geochemical reactions-induced hydrogen loss during underground hydrogen storage in sandstone reservoirs. Int J Hydrogen Energy 2021;46(38):19998–20009. https://doi.org/10.1016/j.ijhydene.2021.03.116.
[36] Zeng L, Keshavarz A, Xie Q, et al. Hydrogen storage in Majiagou carbonate reservoir in China: geochemical modelling on carbonate dissolution and hydrogen loss. Int J Hydrogen Energy 2022;47(59):24861–70. https://doi.org/10.1016/j.ijhydene.2022.05.247.
[37] Truche L, Berger G, Destrigneville C, et al. Kinetics of pyrite to pyrrhotite reduction by hydrogen in calcite buffered solutions between 90 and 180 C: Implications for nuclear waste disposal. Geochem Cosmochim Acta 2010;74(10):2894–914. https://doi.org/10.1016/j.gca.2010.02.027.
[38] Truche L, Jodin-Caumon M-C, Lerouge C, et al. Sulphide mineral reactions in clay-rich rock induced by high hydrogen pressure: application to disturbed or natural

settings up to 250 C and 30 bar. Chem Geol 2013;351:217–28. https://doi.org/10.1016/j.chemgeo.2013.05.025.
[39] Zhang T, Amrani A, Ellis GS, et al. Experimental investigation on thermochemical sulfate reduction by H2S initiation. Geochem Cosmochim Acta 2008;72(14):3518–30. https://doi.org/10.1016/j.gca.2008.04.036.
[40] Bensing JP, Misch D, Skerbisch L, et al. Hydrogen-induced calcite dissolution in Amaltheenton Formation claystones: implications for underground hydrogen storage caprock integrity. Int J Hydrogen Energy 2022;47(71):30621–6. https://doi.org/10.1016/j.ijhydene.2022.07.023.
[41] Al-Yaseri A, Al-Mukainah H, Yekeen N, et al. Experimental investigation of hydrogen-carbonate reactions via computerized tomography: implications for underground hydrogen storage. Int J Hydrogen Energy 2023;48(9):3583–92. https://doi.org/10.1016/j.ijhydene.2022.10.148.
[42] Al-Yaseri A, Al-Mukainah H, Yekeen N. Experimental insights into limestone-hydrogen interactions and the resultant effects on underground hydrogen storage. Fuel 2023;344:128000. https://doi.org/10.1016/j.fuel.2023.128000.
[43] Gelencsér O, Árvai C, Mika L, et al. Effect of hydrogen on calcite reactivity in sandstone reservoirs: experimental results compared to geochemical modeling predictions. J Energy Storage 2023;61:106737. https://doi.org/10.1016/j.est.2023.106737.
[44] Zhan S, Zeng L, Al-Yaseri A, et al. Geochemical modelling on the role of redox reactions during hydrogen underground storage in porous media. Int J Hydrogen Energy 2024;50:19–35. https://doi.org/10.1016/j.ijhydene.2023.06.153.
[45] Ebrahimiyekta A. Characterization of geochemical interactions and migration of hydrogen in sandstone sedimentary formations: application to geological storage. Université d'Orléans. 2017. p. 191.
[46] Yekta AE, Pichavant M, Audigane P. Evaluation of geochemical reactivity of hydrogen in sandstone: application to geological storage. Appl Geochem 2018;95:182–94. https://doi.org/10.1016/j.apgeochem.2018.05.021.
[47] Hassanpouryouzband A, Adie K, Cowen T, et al. Geological hydrogen storage: geochemical reactivity of hydrogen with sandstone reservoirs. ACS Energy Lett 2022;7:2203–10. https://doi.org/10.1021/acsenergylett.2c01024.
[48] Dickson J. A modified staining technique for carbonates in thin section. Nature 1965;205(4971). https://doi.org/10.1038/205587a0. 587-587.
[49] Busch B, Hilgers C, Lander RH, et al. Reservoir quality and burial model evaluation by kinetic quartz and illite cementation modeling: case study of Rotliegendes, north Germany. AAPG (Am Assoc Pet Geol) Bull 2018;102(2):293–307. https://doi.org/10.1306/0503171605217075.
[50] Busch B, Böcker J, Hilgers C. Improved reservoir quality assessment by evaluating illite grain coatings, quartz cementation, and compaction–case study from the Buntsandstein, Upper Rhine Graben, Germany. Geoenergy Sci Eng 2024:213141. https://doi.org/10.1016/j.geoen.2024.213141.
[51] Klinkenberg L. The permeability of porous media to liquids and gases. In: Drilling and production practice. New York: OnePetro; 1941.
[52] Greve J, Busch B, Quandt D, et al. The influence of sedimentary facies, mineralogy, and diagenesis on reservoir properties of the coal-bearing Upper Carboniferous of NW Germany. Petrol Geosci 2024;30(1):20. https://doi.org/10.6084/m9.figshare.c.7003156.v1. petgeo2023.
[53] Tarling D, Hrouda F. Magnetic anisotropy of rocks. London, UK: Chapman and Hall; 1993.
[54] Pearce CI, Pattrick RA, Vaughan DJ. Electrical and magnetic properties of sulfides. Rev Mineral Geochem 2006;61(1):127–80. https://doi.org/10.2138/rmg.2006.61.3.
[55] Busch B, Adelmann D, Herrmann R, et al. Controls on compactional behavior and reservoir quality in a triassic Buntsandstein reservoir, upper rhine graben, SW Germany. Mar Petrol Geol 2022;136:105437. https://doi.org/10.1016/j.marpetgeo.2021.105437.
[56] Folk RL. Petrology of sedimentary rocks. Austin, Texas: Hemphill Publishing Company; 1980.
[57] España JS. The behavior of iron and aluminum in acid mine drainage: speciation, mineralogy, and environmental significance. In: Letcher TM, editor. Thermodynamics, solubility and environmental issues. Elsevier; 2007. p. 137–50. https://doi.org/10.1016/B978-044452707-3/50009-4.
[58] Parkhurst DL, Appelo C. Description of input and examples for PHREEQC version 3—a computer program for speciation, batch-reaction, one-dimensional transport, and inverse geochemical calculations. US Geological Survey Tech Methods 2013;6(A43):497.
[59] Davies SH, Morgan JJ. Manganese (II) oxidation kinetics on metal oxide surfaces. J Colloid Interface Sci 1989;129(1):63–77. https://doi.org/10.1016/0021-9797(89)90416-5.
[60] Schwertmann U. Solubility and dissolution of iron oxides. Plant Soil 1991;130:1–25. https://doi.org/10.1007/BF00011851.
[61] Sánchez-España J, Yusta I, Burgos WD. Geochemistry of dissolved aluminum at low pH: hydrobasaluminite formation and interaction with trace metals, silica and microbial cells under anoxic conditions. Chem Geol 2016;441:124–37. https://doi.org/10.1016/j.chemgeo.2016.08.004.
[62] Saeed M, Jadhawar P. Optimizing underground hydrogen storage in aquifers: the impact of cushion gas type. Int J Hydrogen Energy 2024;52:1537–49. https://doi.org/10.1016/j.ijhydene.2023.08.352.